

Antisite effect on ferromagnetism in (Ga,Mn)As

R. C. Myers,¹ B. L. Sheu,² A. W. Jackson,¹ A. C. Gossard,¹ P. Schiffer,² N. Samarth,² and D. D. Awschalom¹

¹Center for Spintronics and Quantum Computation,
University of California, Santa Barbara, CA 93106.

²Department of Physics and Materials Research Institute,
The Pennsylvania State University, University Park, PA 16802.

(Dated: February 6, 2008)

We study the Curie temperature and hole density of (Ga,Mn)As while systematically varying the As-antisite density. Hole compensation by As-antisites limits the Curie temperature and can completely quench long-range ferromagnetic order in the low doping regime of 1-2% Mn. Samples are grown by molecular beam epitaxy without substrate rotation in order to smoothly vary the As to Ga flux ratio across a single wafer. This technique allows for a systematic study of the effect of As stoichiometry on the structural, electronic, and magnetic properties of (Ga,Mn)As. For concentrations less than 1.5% Mn, a strong deviation from $T_C \propto p^{0.33}$ is observed. Our results emphasize that proper control of As-antisite compensation is critical for controlling the Curie temperatures in (Ga,Mn)As at the low doping limit.

PACS numbers: 75.50.Pp, 75.70.-i, 71.55.Eq, 74.62.Dh

I. INTRODUCTION

In (Ga,Mn)As, currently the most studied dilute magnetic semiconductor (DMS), a long-range ferromagnetic interaction between dilute Mn^{2+} spins is mediated by valence band (or defect band) hole spins.^{1,2,3} Most experimental work in this system has focused on achieving maximal Curie temperatures (T_C 's) in a technological drive to bring ferromagnetism in (Ga,Mn)As to more practical temperatures.⁴ In this vein, it was determined that a crucial limiting parameter of the T_C of as-grown (Ga,Mn)As is the incorporation of hole compensating crystalline defects, which are unintentionally formed due to the low growth temperature ($\sim 250^\circ\text{C}$) and low solubility of Mn in GaAs. One such defect, the Mn interstitial (Mn_i), is considered to be a double donor compensating two holes each.⁵ These defects have shown a surprisingly high diffusivity allowing for their removal by using post-growth annealing at relatively low temperatures ($\sim 200^\circ\text{C}$) that drive them to the surface.⁶ Consequently, the three dimensional hole density (p) and T_C after annealing can be drastically increased.⁷ Another well-studied defect in low temperature (LT) grown GaAs is excess arsenic. For substrate temperatures less than 300°C , excess arsenic is incorporated by occupying a Ga-site, called an antisite defect (As_{Ga}) which - like the Mn_i defect is also a double donor.⁸ The density of these defects can reach 10^{20} cm^{-3} , $\sim 1\%$ of Ga-sites, which is the same order of magnitude as typical Mn doping levels.⁹ By post-growth annealing at temperatures above 500°C , As_{Ga} can be removed by the formation of metallic As precipitates,¹⁰ however at these temperatures Mn also precipitates out of the (Ga,Mn)As solid solution as MnAs nano-particles.¹¹

Most experimental work on (Ga,Mn)As has been aimed at maximizing the T_C by controlling the compensating defects in the high doping regime, i.e. Mn $\sim 5\text{-}9\%$. Such studies mainly focus on the reduction of Mn_i defects through post-growth annealing while loosely treating the

problem of As non-stoichiometry. As_{Ga} defects are usually ignored in the high doping regime since Mn_i defects are the main source of carrier compensation, and their removal has led to dramatic increases in p and T_C .⁷ On the other hand, hole compensation due to As_{Ga} could be as large as 10^{20} cm^{-3} , which would shift T_C in this Mn-doping range by up to 10 K.

In contrast, near the ferromagnetic threshold of $\sim 1\%$ Mn, compensation due to As_{Ga} could dramatically alter the T_C 's since here the defect and dopant densities are roughly equal. Additionally, the concentration of Mn necessary for the onset of ferromagnetism should be a strong function of carrier compensation since the ferromagnetism depends strongly on p ; *in the low doping limit ferromagnetism is likely extrinsically limited by hole compensating defects*. We also note that theoretical work predicts a change in the mechanism of ferromagnetism in the low doping limit, near the insulator-metal transition,^{5,12} compared with the metallic limit at which $T_C \propto p^{0.33}$ as predicted by the Zener-model.²

The effect of excess As on the lattice constant of (Ga,Mn)As was treated by Schott *et al.*,¹³ who used a different As-flux than another study¹⁴ and noted a change in the extrapolated lattice constant of zinc blende MnAs due to As_{Ga} incorporation. They followed-up their study by using 2 different As:Ga beam flux ratios, differing by 500% and noted large changes in the lattice constant of (Ga,Mn)As over a broad range of Mn-doping and substrate temperatures.¹⁵ These results were elaborated upon by Sadowski and Domagala, who measured lattice constant variation in $\text{Ga}_{0.96}\text{Mn}_{0.04}\text{As}$ grown using 3 different As:Ga flux ratios and noted an interplay between Mn_i and As_{Ga} incorporation for this Mn doping regime.¹⁶ Campion *et al.* reported an improvement in structural and magnetic properties of (Ga,Mn)As films grown using As_2 instead of As_4 .¹⁷ Their paper, however, does not describe the fluxes used for each As-species nor how the effective III-V ratio varies between these cases.

The same group has reported impressively high T_C 's over a broad range of Mn-doping levels, mentioning the importance of minimizing the As:Ga flux ratio although no data on the variation of this parameter were provided.¹⁸ Avrutin *et al.* carried out the first study that measured both the structural, electrical, and magnetic properties of (Ga,Mn)As using 2 different As:Ga flux ratios.¹⁹ They noted an optimization of the hole density, conductivity, and T_C for the low As:Ga flux ratio, where fewer As_{Ga} should be incorporated.

In this paper, we present the first systematic investigation of the effect of As_{Ga} incorporation on the structural, electronic, and magnetic properties of (Ga,Mn)As in the low Mn-doping regime. The As:Ga flux ratio is smoothly varied within individual samples by using molecular beam epitaxy (MBE) without substrate rotation. The geometry of the MBE chamber inherently provides a gradient in the As:Ga flux ratio across the substrate of $\pm 50\%$, while maintaining a roughly uniform Mn flux. In order to avoid formation of Mn_i and to achieve a high sensitivity to carrier compensation, we chose Mn doping concentrations of 1 - 2%, in the region of the onset of ferromagnetism. At Mn concentrations less than 1.5%, Mn_i has a larger formation energy than Mn_{Ga}.³ Thus no interstitial Mn will form and all hole compensation should originate from As_{Ga}. Film morphology is measured *in-situ* by reflection high energy electron diffraction (RHEED) and *ex-situ* by atomic force microscopy (AFM). Out-of-plane epitaxial strain is measured by high-resolution x-ray diffraction (HRXRD). Electronic properties at room temperature are measured by Hall effect in the Van der Pauw and Hall-bar geometry, and magnetic properties are measured by SQUID magnetometry (Quantum Design MPMS).

The epitaxial strain due to the incorporation of As_{Ga} can be controlled by the As:Ga flux ratio, as previously reported.^{8,16} More interestingly, the electronic and magnetic properties reveal a strong sensitivity to As_{Ga} compensation with conductivities and hole densities (p) spanning over two orders of magnitude leading to a transition from paramagnetism to ferromagnetism for constant Mn densities (Sec. III and VI). Hole compensation due to As_{Ga} reduces p and therefore T_C . The As:Ga flux ratio is also observed to significantly alter film morphology (Sec. V). In the As-rich condition, films attain maximum smoothness, show a high degree of As_{Ga} related carrier compensation, and exhibit reduced or suppressed Curie temperatures. For As:Ga flux ratios at which the p and therefore T_C are maximized (stoichiometric condition, As_{Ga} ~ 0), the films remain two-dimensional (2D) but are rougher than the As-rich material. In the Ga-rich condition (small As:Ga flux ratios), films become three-dimensional (3D) with the accumulation of excess Ga on the surface leading to an order of magnitude increase in film roughness. At the minimum As:Ga flux ratio investigated, the roughest surfaces are observed with hemispherical Ga-droplets. The group-III enriched surface suppresses Mn incorporation during growth, leading

to lower p and T_C values than in the As-rich condition. In the low Mn-doped regime, where As-compensation limits hole density and ferromagnetic ordering, a strong deviation from the usual $T_C \propto p^{0.33}$ behavior is observed with $T_C \propto p^{0.09}$ for $x \leq 1.5\%$. Our results emphasize that proper control of hole compensation due to As_{Ga} is critical to maximizing the value of T_C 's in the low Mn-doping regime. The combinatorial MBE growth approach used here could be applied to more complex LT grown GaAs-based heterostructures in which the As:Ga flux ratio is a strong control parameter.

II. MOLECULAR BEAM EPITAXY (MBE) GROWTH

All samples are grown on 2-inch diameter GaAs (001) substrates in a Varian Gen-II MBE system manufactured by Veeco Instruments, Inc. with a source to substrate distance of 5.4-inches. The substrate temperature is monitored by absorption band edge spectroscopy (ABES), which measures the substrate temperature in real-time through white-light transmission spectroscopy. The temperature stability during LT (Ga,Mn)As and GaAs growths is typically $\pm 5^\circ\text{C}$. The growth rate of GaAs at the center of the wafer is 0.7 ML/sec as calibrated by RHEED intensity oscillations of the specular spot at 580°C . The Mn doping density is inferred from RHEED intensity oscillation measurements²⁰ of the MnAs growth rate performed at 240°C . Measurements of the Mn density by secondary ion mass spectroscopy (SIMS) indicate that the RHEED calibration underestimates the density by up to 0.4% Mn, which provides a rough error estimate for the quoted Mn concentrations. We use As₂ for all samples presented here, employing a valved cracker/sublimator. The beam equivalent pressure (BEP) of As₂ and Ga are measured with a nude ion gauge at the center position of the substrate just prior to growth. The ratio of As₂ and Ga BEPs, defined as $As : Ga$, is proportional to the ratio of the atomic fluxes of As and Ga delivered to the growing surface. Unfortunately, a reliable quantitative conversion from BEP to atomic flux is difficult due to the uncertainties in the ionization efficiencies of each beam species.²¹ A rough estimate gives that the atomic flux ratio is 2.5 times smaller than the BEP ratios, where we assume that only As₂ are present with a temperature equal to that of the cracking zone.

The following procedure is used for both non-rotated and rotated growths prior to deposition of the low temperature (LT) films. The wafer is first heated to 635°C with $As : Ga \sim 35$ for oxide desorption, monitored by RHEED, and subsequently cooled to 585°C . While rotating at 10 RPM, a 300-nm GaAs buffer layer is grown using 5-s growth interrupts for every 15 nm of deposition resulting in a streaky 2×4 surface reconstruction RHEED pattern. While cooling the substrate to 250°C , the As-valve setting is reduced at 400°C for the desired

$As : Ga$ value for LT growth. Prior to LT growth, a streaky 4×4 surface reconstruction is observed in the RHEED pattern. For rotated growths, once the substrate stabilizes at 250°C the LT growth begins. For non-rotated growths, the substrate rotation is stopped at 400°C and the wafer $[110]$ crystal axis (perpendicular to the wafer major flat) is aligned along the $As : Ga$ gradient direction (y-axis). This can be reproducibly accomplished noting the radial angle between the RHEED e-beam and substrate, fixed by the MBE chamber geometry, and finding a high symmetry crystal axis from the surface reconstruction pattern. All LT films are 100-nm thick at the center wafer position. After completion of the LT layer, they are cooled in a consistent manner to room temperature.

III. ROTATED (Ga,Mn)As: CARRIER COMPENSATION AND QUENCHED FERROMAGNETISM

We first consider the case of rotated growth, examining the effect of Mn concentration and $As : Ga$ on the electronic and magnetic properties. Four samples are grown with the same Mn concentration (2.3%), but with various $As : Ga$. Hole density data are from samples measured in the Van der Pauw geometry in a magnetic field up to 0.2 T. Figure 1a plots p and T_C of these samples as a function of $As : Ga$. Values of T_C are obtained from magnetization versus temperature scans as shown in Fig. 1d selecting the point of maximum second derivative in $M(T)$. The scans are performed during a field warm (50 Oe) after a field cool (1 T). The hole density decreases exponentially with the $As : Ga$, indicating that excess As in the form of As_{Ga} donors are compensating Mn_{Ga} acceptors. Correspondingly, T_C decreases with p , and for $As : Ga \geq 18$ ferromagnetism is suppressed. This strong compensation effect is due to the fact that the As_{Ga} donor and Mn_{Ga} acceptor densities are similar in magnitude in this low Mn-doping regime, $Mn < 2\%$.

Using $As : Ga = 10.3$, for which the largest p and T_C are obtained (Fig. 1a), a series of four additional samples are grown with varying Mn concentration. For this series, variation in p and T_C occurs due to the varying concentration of Mn_{Ga} , Fig. 1b. Clearly the hole density does not increase linearly with Mn concentration, which is indicative of a carrier compensation threshold. Based on this observation, a more careful optimization of $As : Ga$ is necessary, as discussed in the next sections.

Figure 1c plots T_C as a function of p , summarizing data from Fig. 1a and b. We observe that varying the concentration of compensating As_{Ga} donors (by varying $As : Ga$) has a qualitatively identical effect as varying the concentration of magnetic Mn_{Ga} acceptors with respect to the carrier density and magnetic transition temperature. A fit of $T_C \propto p^{0.33}$ to the ferromagnetic samples in Fig. 1c, Mn doping $\geq 1.5\%$, reveals the usual functional dependence.⁴

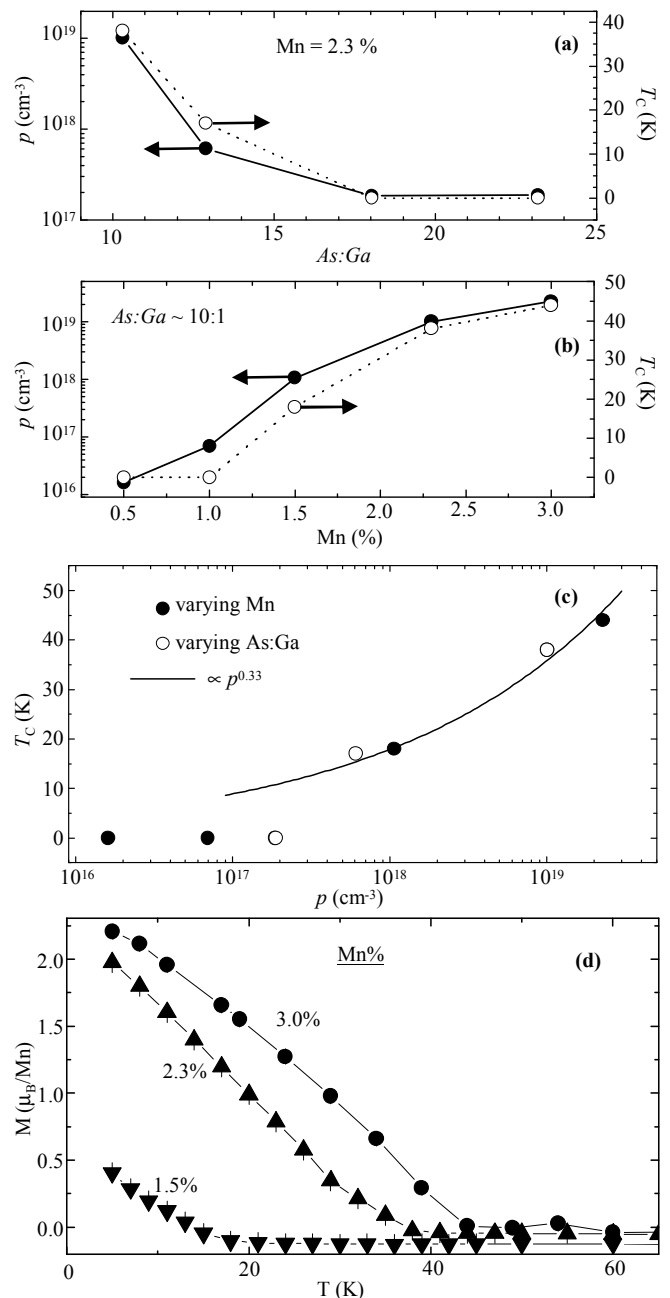


FIG. 1: Quenched ferromagnetism by As-compensation. Data from (Ga,Mn)As films grown at 250°C using substrate rotation. (a) Samples were grown using a constant growth rate and Mn concentration but varying $As : Ga$. Room temperature hole density (p) is plotted on the left vertical axis as a function of $As : Ga$. The corresponding Curie temperature (T_C) is plotted on the right vertical axis. (b) Similar data plotted for samples grown with a constant $As : Ga$, but varying Mn concentration. (c) Data in (a) and (b) are replotted with T_C as a function of p . A fit to $T_C \propto p^{0.33}$ is shown for the ferromagnetic samples. (d) Magnetization versus temperature scans (field-warmed with $B = 50$ Oe) used to extract T_C shown in (b).

IV. NON-ROTATED (GA,MN)AS: COMBINATORIAL VARIATION OF $As : Ga$

In order to systematically study the effect of the excess As on the electronic and magnetic properties of (Ga,Mn)As, we use a method of non-rotated growth in which the geometry of the MBE system provides a continuous variation in $As : Ga$ across the wafer.²² Thus the advantage of a combinatorial approach is employed in which a single non-rotated growth provides the equivalent of twenty rotated growths of various $As : Ga$. The phase space of $As : Ga$ and Mn concentration can be mapped-out in high-resolution while performing a much smaller number of growths than otherwise required.

Figure 2a schematically shows the position of the Ga Knudsen cell and the As valved-cracker/sublimator relative to the substrate position. The angle between the Ga and As_2 molecular beams provides a continuous variation in $As : Ga$ across the y-axis of the substrate, as defined in the schematic. The variation of the As flux is measured by depositing a thick As film on a quartz wafer, covered by a shadow mask along the y-axis, with the substrate stabilized below room temperature. We have assumed that the deposition rate of As under these conditions is proportional to the As flux. A profilometer is used to measure the thickness of the As film along the y-axis. The normalized flux variation of As, plotted in Fig. 2b, is calculated by normalizing the thickness along y by the thickness at $y = 0$. The variation of the Ga-flux is measured using an optical measurement of a distributed Bragg reflector (DBR) and cavity structure grown in 2 separate steps. First, a 10 period GaAs/AlGaAs DBR is grown on a rotated 2-inch substrate in a larger, more uniform system (Veeco Gen III) with a source to substrate distance of 11-inches. This results in an extremely uniform DBR which is As-capped and transferred into the Gen II system. The As-cap is desorbed and a GaAs optical cavity layer is grown on the sample without substrate rotation. The reflectance spectrum of the sample is measured *ex-situ* at different points across the wafer and is fit to an optical model of the reflectance. Because the 10 period DBR was almost completely uniform, the thickness of the non-uniform GaAs layer grown in the Gen II could be accurately and unambiguously determined by fitting the measured optical spectrum to a computer model of the structure. Since the deposition is performed at 585 °C, the growth rate is independent of the As overpressure, being limited by the group-III flux only. The normalized Ga rate, proportional to the Ga-flux, along the y-axis is plotted in Fig. 2b. Both the As and Ga flux variation are well fit by a second order polynomial (lines), which are used to convert y-axis position for non-rotated growths to $As : Ga$.

Next we consider the Mn flux variation across the substrate. Since the Mn Knudsen cell is roughly perpendicular to the y-axis, variation along this direction is expected to be small. In order to measure the Mn variation across the substrate, a 1- μ m thick GaAs:Mn layer with Mn ~

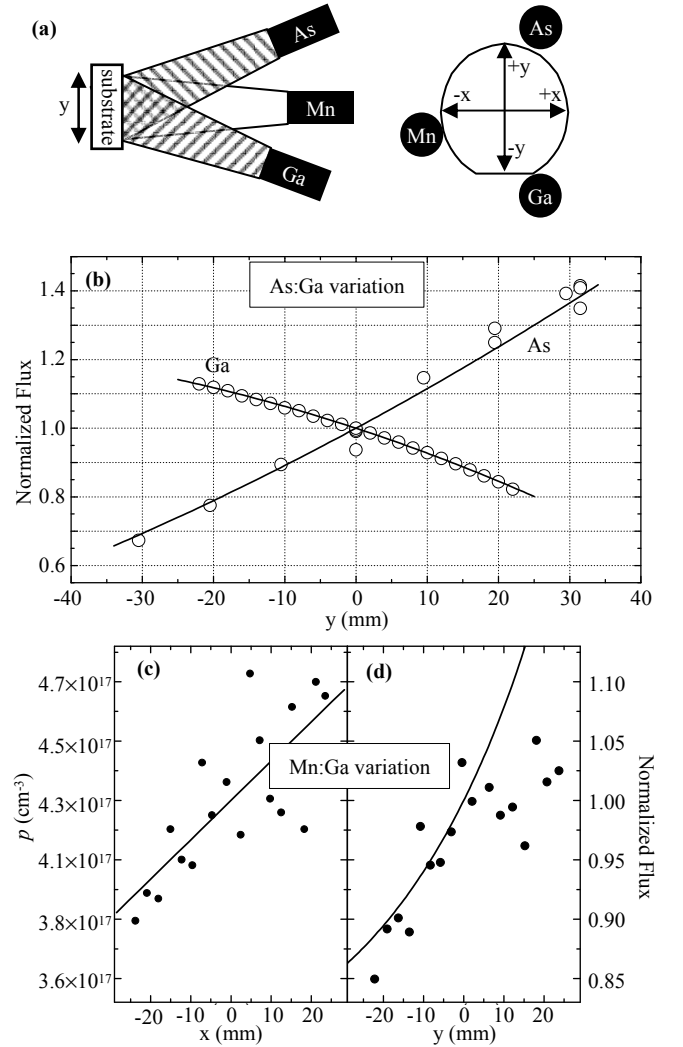


FIG. 2: Geometric flux gradients in the MBE system. $As : Ga$ is continuously varied and optimized in a single non-rotated growth. (a) Deposition geometry (not to scale) in the MBE system. The relative positions of the As, Ga, and Mn Knudsen cells with respect to the substrate are shown from side and front views. (b) The flux gradient of Ga and As molecular beams along the y-axis of the wafer normalized to the center flux value. Measured values (data points) and fits to second order polynomials (lines) are shown. (c)-(d) The Mn:Ga flux variation along the x-axis (c) and y-axis (d) of the wafer measured from hole density (p) variation in non-rotated samples grown at 400 °C, where As-flux does not affect carrier density. The line in (d) is the inverse of the Ga-flux variation, shown as a line in (b), which accounts for the variation in the Mn:Ga ratio along the y-axis.

$4 \times 10^{17} \text{ cm}^{-3}$ is deposited at 400 °C with an As_2 overpressure. At these conditions Mn incorporation is fully substitutional and excess As incorporation is negligible ($< 1 \times 10^{16} \text{ cm}^{-3}$), thus the hole density is proportional to the Mn:Ga flux ratio.²³ The hole density variation across the x and y axes due to Mn:Ga variation is plotted in Fig. 2 c and d, respectively. Along either axis, the

Mn:Ga ratio varies by 5-10%, which would correspond to variation in the Mn concentrations of 0.05 to 0.1%. As will be clear (Sec. VI), this variation in Mn concentration is negligible with respect to the As compensation effect under investigation.

V. FILM MORPHOLOGY AND STRAIN VERSUS $As : Ga$

To study the effect of $As : Ga$ on the film morphology, the RMS roughness of non-rotated samples is measured across the y-axis by AFM. We describe results from two non-rotated films, without Mn doping and with 1.5% Mn. Both $5 \times 5\text{-}\mu\text{m}^2$ and $1 \times 1\text{-}\mu\text{m}^2$ area scans are measured every 3 to 4 mm along the y-axis of both wafers. The RMS roughness from these scans is plotted as a function of $As : Ga$ (converted from y-position from Fig. 2b calibration) and representative AFM images of each region are shown in Fig. 3.

In the As-rich region from $11 < As : Ga < 14$, AFM images reveal fully coalesced films with RMS roughness of 0.2 nm or less indicative of a 2D growth mode. RHEED observations of such films, from rotated growths at the same $As : Ga$ condition, show sharp and streaky 2D reconstruction. In the As-rich to stoichiometric region from $9 < As : Ga < 11$, films show a nanoscale-granular structure. For decreasing $As : Ga$, this granular structure becomes more distinct and the film roughness increases, however it remains below 1 nm RMS. RHEED observations for films grown in this $As : Ga$ range show a spotty reconstruction pattern indicative of a rough, but 2D surface, which we have found to be characteristic of films near the stoichiometric condition. In this region, the hole density of Mn-doped films reaches a maximum indicating the minimum of compensating As_{Ga} defects (Sec. VI).

Just below $As : Ga \sim 9$, the RMS film roughness increases by a factor of ten as $As : Ga$ transitions from the stoichiometric condition to Ga-rich. AFM images of this region show the formation of 10-nm tall clover-shaped features 60-nm in diameter with a crater in the center. The RHEED pattern of these films shows additional spots indicative of 3D features on the surface. For $As : Ga < 9$, the surface roughness continues to increase with the appearance of larger droplet-like features. At the lowest $As : Ga$ ratio, these hemispherical droplets are 50-nm tall and 240-nm in diameter. The large change in roughness across the non-rotated wafers is observable by eye under intense illumination, where the surface transitions from mirror finish at the As-rich region to a hazy surface in the Ga-rich region.

As observed in the roughness plot of Fig. 3, it appears that Mn-doping suppresses the onset of roughening toward smaller $As : Ga$. In contrast, since Mn-doping increases the effective group-III flux, one would expect a shift in the onset of roughness to higher $As : Ga$. This smoothing may be due to a surfactant effect of Mn on the surface. As discussed in Sec. VI, the highest hole densi-

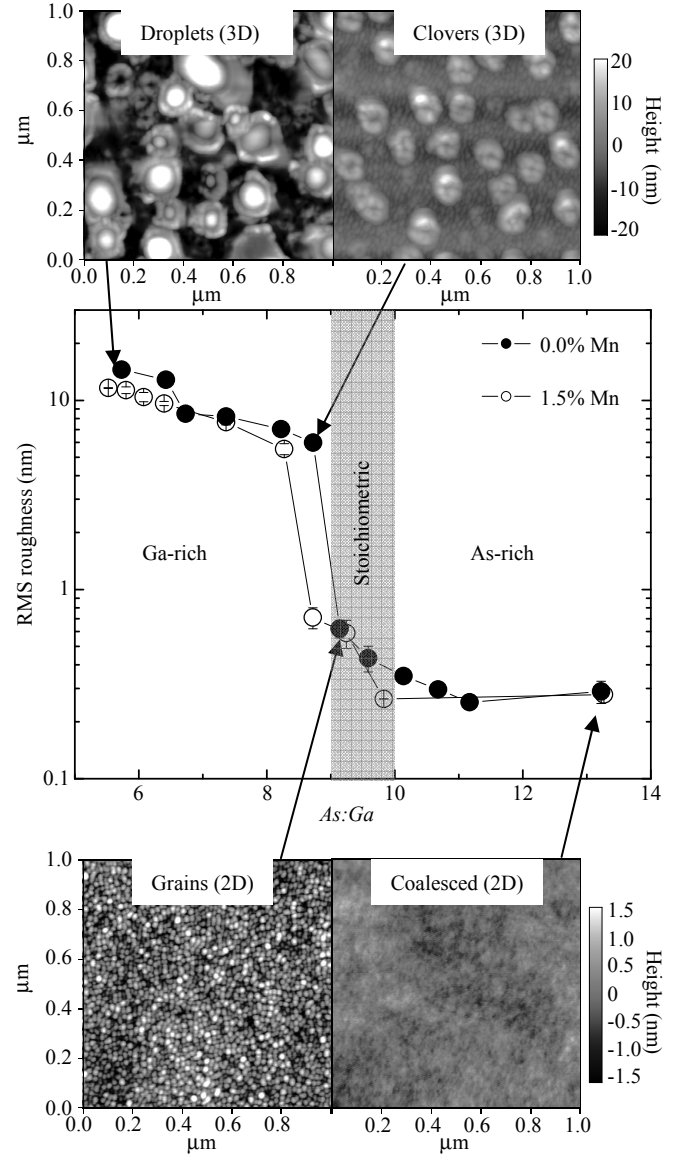


FIG. 3: Morphology of GaAs and (Ga,Mn)As films as a function of $As : Ga$ (non-rotated growths). AFM micrographs ($1 \times 1\text{ }\mu\text{m}^2$ scans) are plotted for a GaAs growth, but are qualitatively identical to (Ga,Mn)As films in the same wafer position. The RMS roughness measured from such AFM scans is plotted as a function of $As : Ga$ (along y-axis of wafer) for both a GaAs and (Ga,Mn)As sample. The stoichiometric region is shaded grey, where excess As is minimized, two-dimensional growth (2D) is maintained, however, some granular structure is observed.

ties are observed in (Ga,Mn)As grown with $As : Ga$ just before the transition from 2D to 3D surface, indicating that the growth kinetics at this stoichiometric condition do not significantly increase the density of hole compensating Mn_i donors.

HRXRD scans are obtained using a triple-axis (Phillips X'Pert MRD Pro) thin film diffractometer. We measure ω - 2θ scans near the (004) Bragg peak of the (001)

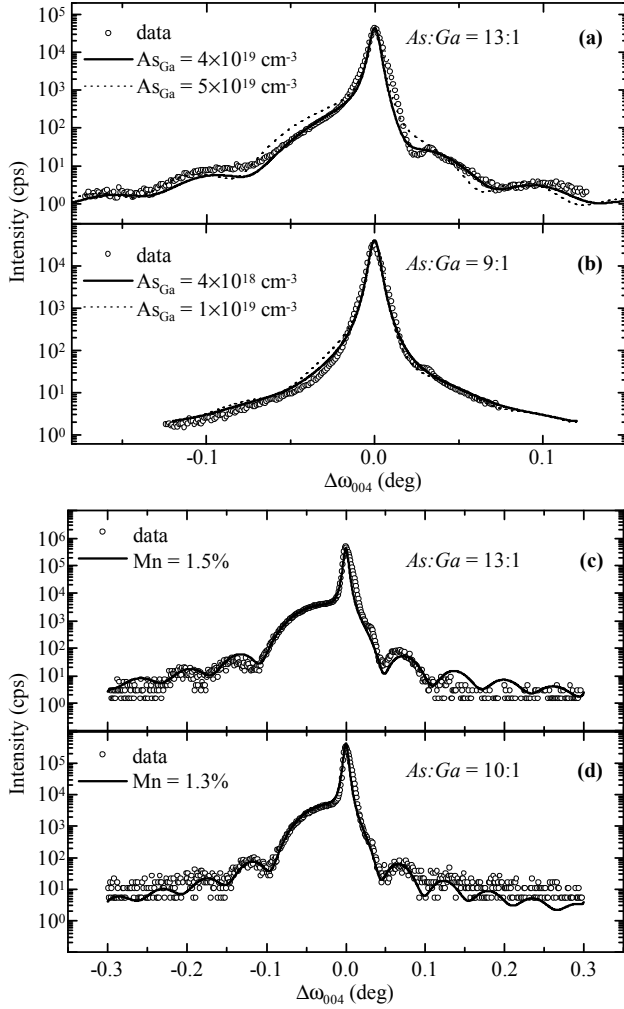


FIG. 4: Film strain due to As non-stoichiometry and Mn incorporation in GaAs and (Ga,Mn)As non-rotated films measured by ω -2 θ HRXRD scans near the (004) peak. (a)-(b) Data from a GaAs film at the As-rich wafer position (a) and stoichiometric position (b). Data (points) and dynamical simulations (lines) are plotted for various As_{Ga} densities. (c)-(d) Data from a (Ga,Mn)As film at the As-rich wafer position (c) and stoichiometric position (d). Data (points) and dynamical simulations (lines) are plotted using different Mn densities.

GaAs substrate. The diffraction patterns obtained for the non-rotated LT GaAs film at the position of highest As-compensation ($\text{As} : \text{Ga} = 13 : 1$) and at the stoichiometric condition ($\text{As} : \text{Ga} = 9 : 1$) are plotted in Fig. 4 a and b, respectively. In the As-rich position, the epilayer peak appears as a shoulder at lower angle, reflecting the increase in the out-of-plane lattice constant, due to As_{Ga} incorporation. We also note the thickness fringes indicative of the high quality of the film surface and interface. A dynamical HRXRD program is used to simulate the data²⁴ assuming that the lattice constant of $(\text{Ga}_{1-z}, \text{As}_z)\text{As}$, $a = 5.654 + 1.356z$.⁸ Best fit simulations in Fig. 4a give a film thickness 90 nm and $\text{As}_{\text{Ga}} = 4 \times 10^{19} \text{ cm}^{-3}$. The additional fit with $\text{As}_{\text{Ga}} = 5 \times 10^{19} \text{ cm}^{-3}$

shows the error in the As_{Ga} estimate is about $1 \times 10^{19} \text{ cm}^{-3}$. The thickness of the epilayer is 10-15% thinner at the top edge than at the center of the wafer due to the smaller Ga-flux at this position, as shown in Fig. 2b. At the stoichiometric position the epilayer shoulder becomes small, only visible as a slight asymmetry on the left side of the substrate diffraction peak in Fig. 4b. Simulations using a film thickness of 100 nm yield $\text{As}_{\text{Ga}} = 4 \times 10^{18} \text{ cm}^{-3}$, which is smaller than the uncertainty of the fits. A more precise estimate of the As_{Ga} density is found from the hole density variation, discussed in Sec. VI. Thickness fringes disappear since the lattice constant of the epilayer is almost indistinguishable from that of the substrate.

Figure 4 c and d plot the diffraction patterns from a non-rotated (Ga,Mn)As film with 1.5% Mn from the As-rich and stoichiometric positions, respectively. For these layers, strain due to Mn incorporation dominates the epilayer lattice constant obscuring the As_{Ga} effect. Simulations are performed assuming that the lattice constant of $(\text{Ga}_{1-x}, \text{Mn}_x)\text{As}$, $a = 5.654 + 0.476x$.¹³ The fits indicate a film thickness of 85 nm and 95 nm, and Mn concentration of 1.5% and 1.3% at the As-rich and stoichiometric positions, respectively. The variation in Mn concentration is not explained by the Mn:Ga ratio variation along y, Fig. 2d, which would predict a decrease in Mn concentration of up to 0.1%. The additional strain reduction may be due to the minimization of As_{Ga} defects at the stoichiometric position, but the uncertainty of the HRXRD simulations prevents a more quantitative analysis.

VI. CARRIER DENSITY AND CURIE TEMPERATURE VERSUS $\text{As} : \text{Ga}$

A. Hole density gradient

Figure 5 a and b show the variation in hole density for a series of non-rotated (Ga,Mn)As films of various Mn concentrations (a) along the y-axis, and (b) with y converted to $\text{As} : \text{Ga}$, using the Fig. 2b calibration. All the hole density data in the figures are from room temperature measurements of samples prepared in the Van der Pauw geometry ($3 \times 3 \text{ mm}^2$) in a magnetic field up to 0.2 T. Selective measurements of the hole density of patterned Hall-bars in magnetic fields up to 2 T agree with the Van der Pauw measurements to within 50%. Additional high field measurements at 7-9 T deviate from the low field data by up to 50 %.

The hole density varies by over two orders of magnitude across each wafer showing a maximum value near $y \sim 6 \text{ mm}$ corresponding to $\text{As} : \text{Ga} \sim 9$. The results are explained by a decreasing number of As_{Ga} donors that compensate Mn_{Ga} acceptors as $\text{As} : \text{Ga}$ is reduced from the As-rich condition. The maximum of p along y corresponds to the position at which As_{Ga} are minimized, the stoichiometric condition. A further reduction

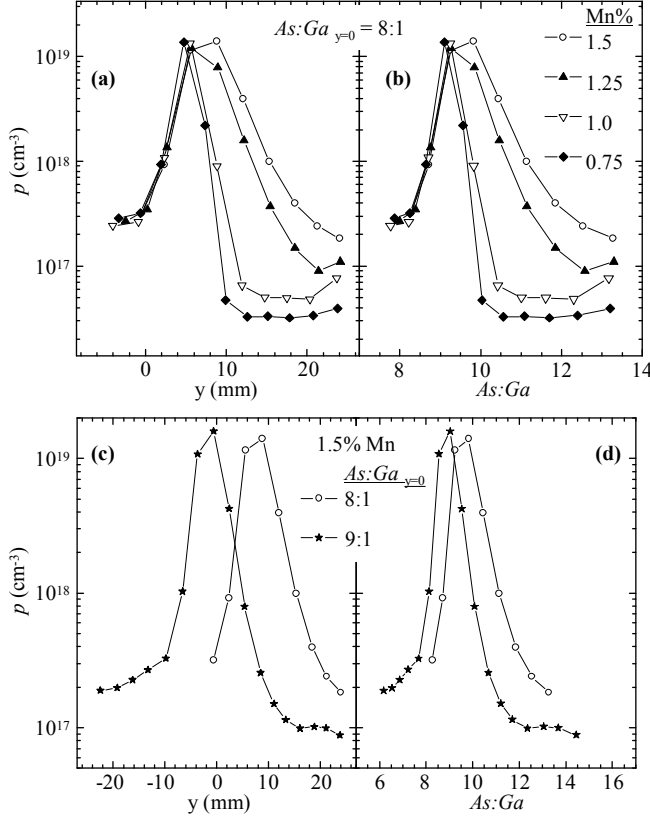


FIG. 5: The As-compensation gradient in non-rotated (Ga,Mn)As films. The room temperature hole density (p) variation along films grown with different Mn concentrations, (a) as a function of y -position, and (b) as a function of $As : Ga$. (c)-(d) Similar data for samples with the same Mn concentrations but different $As : Ga$ at $y = 0$. Lines in each plot connect data points from the same wafer.

in $As : Ga$ leads to a Ga-rich surface that limits Mn incorporation, and leads to a ten-fold increase in surface roughness marking a transition from 2D to 3D film morphology (Sec. V). The y -position of the maximum in p matches in four separate non-rotated growths demonstrating the reproducibility of this technique. When the Mn density is reduced, the hole-density peak narrows on the As-rich side, indicating that samples with lower Mn-doping density are more sensitive to the As_{Ga} compensation effect. This follows if $As : Ga$ controls the density of hole compensating defects independently from the doping density of Mn, as expected for this doping regime.

We note that for the 0.75% Mn doped wafer, when $As : Ga \sim 10$ the hole compensation is nearly complete, $p \sim 10^{16} \text{ cm}^{-3}$. For $As : Ga \sim 9$, the compensation is minimized, $p \sim 10^{19} \text{ cm}^{-3}$. In this case, a 10% reduction in $As : Ga$ reduces the As_{Ga} compensation by three orders of magnitude. This demonstrates the strong sensitivity of the As_{Ga} incorporation to $As : Ga$, and the high degree of As-flux control, within 10%, necessary to properly minimize this defect. Previous studies of the

effect of $As : Ga$ ratio reported only two or three values of this parameter in increments of 200% or more.^{15,16,19}

In the Ga-rich position ($As : Ga < 9$), the hole density decreases along with $As : Ga$, but remains constant as the Mn doping density is varied, Fig. 5b. This behavior is explained by a solubility limit for Mn, which is below any of the Mn doping levels used here. Decreasing $As : Ga$ below the stoichiometric value leads to a Ga-rich surface that serves as a kinetic barrier for the incorporation of group-III substitutional dopants, such as Mn. One might consider the alternative possibility that interstitial incorporation of Mn might occur in these circumstances and could explain the reduction in hole density in the Ga-rich region. However, if Mn_i donors were incorporating and compensating the Mn_{Ga} acceptors, then the carrier density should change as the Mn-doping density is altered, which is not the case here. Preliminary SIMS data show a decreasing concentration of Mn in the Ga-rich region as the thickness increases, whereas the As-rich region reveals a relatively constant Mn depth profiles throughout the Mn-doped layer. In the Ga-rich region the Mn density can be $\sim 10^{20} \text{ cm}^{-3}$ lower than in the As-rich region.

The position of the hole density peak can be controlled by adjusting $As : Ga$ at $y = 0$, which shifts the position of the stoichiometric condition along y . To demonstrate this, two wafers with identical Mn concentration of 1.5 % are grown but with different $As : Ga$ at $y = 0$. The variation of p along y is plotted in Fig. 5c. By increasing $As : Ga$ at $y = 0$ from 8:1 to 9:1, the peak position (stoichiometric condition) is shifted by $\sim 1 \text{ cm}$ toward the center of the wafer in a direction away from the As source. This shift is observable by eye as a change in the position of the transition region, where the surface changes from mirror finish to hazy. Converting the y -position to $As : Ga$ should fully overlap the hole density peaks, Fig. 5d. The peaks do not completely overlap indicating that additional factors must be considered, such as the variation in the growth rate across non-rotated wafers, which may play a role in the density of compensating As_{Ga} defects. In the present analysis we have considered only the effect of $As:Ga$.

Finally, we compare samples of equal Mn doping density grown with and without rotation. The hole densities of the rotated samples, Fig. 1b, match the hole densities for the non-rotated samples with similar Mn doping in the As-rich condition of $As : Ga \sim 10.5$, Fig. 5b. This indicates that the rotated sample set, presented in Fig. 1b, is grown under a slightly As-rich condition, on the right side of the hole density peak of Fig. 5b.

B. Curie temperature gradient

The Curie temperature variation with $As : Ga$ for two non-rotated (Ga,Mn)As films is plotted in Fig. 6 a and b, together with the hole density variation. T_C is determined from scans similar to those plotted in Fig. 1d. T_C tracks the p variation with $As : Ga$, displaying a maxi-

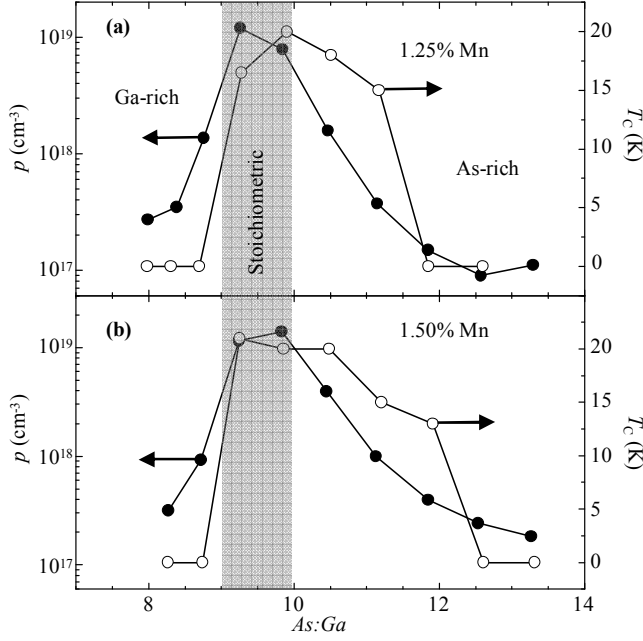


FIG. 6: The Curie temperature gradient in non-rotated (Ga,Mn)As films due to As-compensation. The hole density (p) and T_C are plotted as a function of $As : Ga$ for two wafers with different Mn concentrations, (a) 1.25%, and (b) 1.50%. Lines guide the eye. The stoichiometric region is shaded grey, where excess As is minimized.

mum in Curie temperature in the same region where the hole density peaks. In the As-rich portion of the wafer, As_{Ga} donors limit the hole density and therefore T_C . This effect is very clear, for example, with $As : Ga > 12$, where ferromagnetism is completely suppressed in both 1.5% and 1.25% samples due to hole compensation from As non-stoichiometry in the form of As_{Ga} donors.

The width and shape of the T_C and hole density peaks are quite different. In general, the T_C peaks are wider than the hole density peaks on the As-rich side, but are sharper than the hole density peak on the Ga-rich side of the wafer. To explain this behavior, we replot data from several of the non-rotated (Ga,Mn)As wafers to examine the dependence of T_C on the hole density. This dependence is plotted for the As-rich region ($As : Ga \geq 9$) in Fig. 7a, and for the Ga-rich region ($As : Ga \leq 9$) in Fig. 7b.

In the As-rich region, ferromagnetism is observed over a broad range in hole density from 10^{17} to 10^{19} cm^{-3} . For Ga-rich material, however, ferromagnetism is not observed over the same large range in hole densities where ferromagnetism is observed in the As-rich material, shaded grey. As described in Sec. V and VIA, hole density and film morphology measurements indicate that in the Ga-rich region Mn solubility is limited to well-below the level required for ferromagnetism, $< 0.5 \%$. This is probably due to the kinetic disadvantage of a group-III dopant on a heavily Ga-rich surface because of

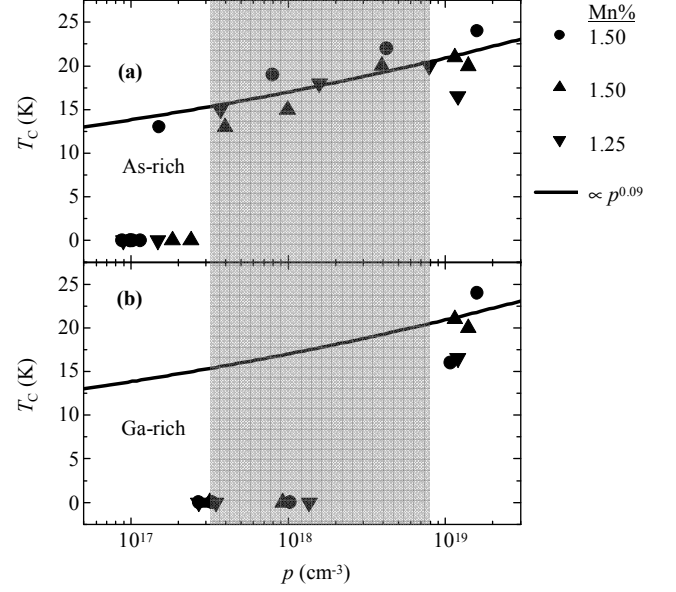


FIG. 7: Curie temperature (T_C) versus hole density (p) in several non-rotated (Ga,Mn)As films showing deviation from $p^{0.33}$. (a) Data are plotted from the As-rich region of the wafer ($As : Ga \geq 9$), and (b) from the Ga-rich region ($As : Ga \leq 9$). The shaded region marks p -values at which ferromagnetism is observed in As-rich material (a) and not in Ga-rich material (b). The line fit of data in (a) to $T_C \propto p^{0.09}$ is replotted in (b).

out-competition. The discrepancy in Fig. 7 between the Ga-rich region and As-rich region offers further support for this hypothesis. In this interpretation, Ga-rich conditions limit Mn_{Ga} to low doping densities of less than 10^{19} cm^{-3} ($< 0.05 \%$ Mn). Whereas for similar hole densities in the As-rich material $Mn_{Ga} \sim 10^{20} \text{ cm}^{-3}$ ($\sim 1 \%$ Mn). Thus ferromagnetism is possible in the As-rich material since there are sufficient Mn_{Ga} acceptors, but the T_C is limited by hole compensation due to As_{Ga} donors. In the Ga-rich material, As_{Ga} compensating donors are not present, but the Mn_{Ga} density is well below the ferromagnetic limit.

The data in Fig. 7a for which $T_C \neq 0$ are fit to $T_C \propto p^{0.09}$ (line). This fit describes the data from two non-rotated wafers with Mn = 1.5% (Fig. 5c) and one wafer with 1.25% Mn over a large range in p and T_C , over 13 data points. In the rotated growths presented in Fig. 1, $p^{0.33}$ behavior is observed for samples with $\geq 1.5 \%$ Mn. There is no discrepancy between the non-rotated and rotated (Ga,Mn)As films if we conjecture that a change in the exponent from 0.33 to 0.09 occurs as the doping is reduced below 1.5% Mn. Since these doping levels are close to the ferromagnetic limit, a change in the dependence of ferromagnetism is not unexpected. The impurity band is fully merged with the valence band in the metallic region of high Mn-doping, where the $p^{0.33}$ is observed. But

at low Mn-doping levels close to the insulating regime, the impurity band is separated from the valence band (Mott gap) where a disorder-based model of ferromagnetism is probably more accurate.¹² Erwin and Petukhov predicted that a strong deviation from the metallic behavior of $T_C \propto p^{0.33}$ should occur in the low Mn-doping regime, $\sim 1.5\%$ Mn, with T_C reaching a maximum in a partially compensated condition (lower p) and ferromagnetism disappearing for zero compensation (highest p); their model assumed that compensation was due to Mn_i alone.⁵ This behavior is not clearly seen in our data, however the observed As_{Ga} compensation was not treated in the model of Erwin and Petukhov.

VII. CONCLUSIONS

The electronic and magnetic properties of (Ga,Mn)As reveal a strong sensitivity to As_{Ga} donors that compensate Mn_{Ga} acceptors. By varying $As : Ga$, the hole densities of (Ga,Mn)As films are varied by more than two orders of magnitude, and, as a result, ferromagnetism can be enhanced or completely suppressed. For As-rich growth, films show the maximum smoothness, but lowest p and T_C . If $As : Ga$ is reduced, the film roughness increases up to the stoichiometric condition, where p and T_C are maximized. For Ga-rich growth, the film roughness increases by an order of magnitude as excess Ga accumulates on the surface. The group-III rich surface suppresses substitutional Mn incorporation leading

to lower p and T_C values than in the As-rich condition. In the low Mn-doped regime, where As-compensation limits hole density and ferromagnetic ordering, a strong deviation from the usual $T_C \propto p^{0.33}$ behavior is observed with $T_C \propto p^{0.09}$ for $x < 1.5\%$. This dependence applies equally well to stoichiometric (Ga,Mn)As as it does to heavily As_{Ga} compensated (Ga,Mn)As. This change in the hole density dependence of T_C occurs in the doping region where the effects of a Mott gap and disorder are expected to alter the mechanism of ferromagnetism.^{5,12} Our results emphasize that precise control of hole compensation due to As_{Ga} is critical to maximizing the value of T_C 's in the low Mn-doping regime. The combinatorial MBE growth approach used here could be applied to more complex LT grown GaAs-based heterostructures in which $As : Ga$ is a strong control parameter. The rapid and high-resolution mapping of growth parameter phase-space by this technique allows for systematic investigations not practicable using more traditional methods.

Acknowledgments

The authors thank D. W. Steuerman for SEM assistance, M. Poggio for helpful criticism, and J. H. English for MBE technical know-how. This work was financially supported by DARPA, ONR, and the NSF. We made use of MRL Central Facilities supported by the MRSEC Program of the NSF (DMR05-20415).

-
- ¹ H. Ohno, Science **281**, 951 (1998).
 - ² T. Dietl, H. Ohno, F. Matsukura, J. Cibert, and D. Fermand, Science **287**, 1019 (2000).
 - ³ T. Jungwirth, J. Sinova, J. Masek, J. Kucera, and A. H. MacDonald, cond-mat/0603380.
 - ⁴ A. H. MacDonald, P. Schiffer, and N. Samarth, Nature Materials **4**, 195 (2005).
 - ⁵ S. C. Erwin and A. G. Petukhov, Phys. Rev. Lett. **89**, 227201 (2002).
 - ⁶ K. W. Edmonds, P. Boguslawski, K. Y. Wang, R. P. Campion, S. N. Novikov, N. R. S. Farley, B. L. Gallagher, C. T. Foxon, M. Sawicki, T. Dietl, M. B. Nardelli, and J. Bernholc, Phys. Rev. Lett. **92**, 037201 (2004).
 - ⁷ K. C. Ku, S. J. Potashnik, R. F. Wang, S. H. Chun, P. Schiffer, N. Samarth, M. J. Seong, A. Mascarenhas, E. Johnston-Halperin, R. C. Myers, A. C. Gossard, and D. D. Awschalom, Appl. Phys. Lett. **82**, 2302 (2003).
 - ⁸ X. Liu, A. Prasad, J. Nishio, E. R. Weber, Z. Liliental-Weber, and W. Walukiewicz, Appl. Phys. Lett. **67**, 279 (1995).
 - ⁹ M. Missous and S. O'Hagan, J. Appl. Phys. **75**, 3396 (1994).
 - ¹⁰ D. E. Bliss, W. Walukiewicz, J. W. Ager III, E. E. Haller, K. T. Chan, and S. Tanigawa, J. Appl. Phys. **71**, 1699 (1992).
 - ¹¹ J. De Boeck, R. Oesterholt, A. Van Esch, H. Bender, C. Bruynseraede, C. Van Hoof, and G. Borghs, Appl. Phys. Lett. **68**, 2744 (1996).
 - ¹² S. R. E. Yang and A. H. MacDonald, Phys. Rev. B **67**, 155202 (2003).
 - ¹³ G. M. Schott, W. Faschinger, and L. W. Molenkamp, Appl. Phys. Lett. **79**, 1807 (2001).
 - ¹⁴ H. Ohno, A. Shen, F. Matsukura, A. Oiwa, A. Endo, S. Katsumoto, and Y. Iye, Appl. Phys. Lett. **69**, 363 (1996).
 - ¹⁵ G. M. Schott, G. Schmidt, G. Karczewski, L. W. Molenkamp, R. Jakiela, A. Barcz, and G. Karczewski, Appl. Phys. Lett. **82**, 4678 (2003).
 - ¹⁶ J. Sadowski and J. Z. Domagala, Phys. Rev. B **69**, 075206 (2004).
 - ¹⁷ R. P. Campion, K. W. Edmonds, L. X. Zhao, K. Y. Wang, C. T. Foxon, B. L. Gallagher, and C. R. Staddon, J. Cryst. Growth. **247**, 42 (2003).
 - ¹⁸ C. T. Foxon, R. P. Campion, K. W. Edmonds, L. Zhao, K. Wang, N. R. S. Farley, C. R. Staddon, and B. L. Gallagher, J. Mater. Sci. - Mater. Elec. **15**, 727 (2005).
 - ¹⁹ V. Avrutin, D. Humienik, S. Frank, A. Koeder, W. Schoch, W. Limmer, R. Sauer, and A. Waag, J. Appl. Phys. **98**, 023909 (2005).
 - ²⁰ F. Schippan, M. Kastner, L. Daweritz, and K. H. Ploog, Appl. Phys. Lett. **76**, 834 (2000).
 - ²¹ R. A. Kubiak, S. M. Newstead, and P. Sullivan, in *Molecular Beam Epitaxy: Applications to Key Materials*, edited by R. F. C. Farrow, (Noyes, 1995).
 - ²² A. W. Jackson, R. C. Myers, and A. C. Gossard, (unpub-

lished).

- ²³ M. Poggio, R. C. Myers, N. P. Stern, A. C. Gossard, and D. D. Awschalom, Phys. Rev. B **72**, 235313 (2005).
- ²⁴ O. Brandt, P. Waltereit, and K. H. Ploog, J. Phys. D -

Appl. Phys. **35**, 577 (2002). “MadMax” executable program courtesy of Patrick Waltereit of Fraunhofer IAF.